Forward scattering in the $H+D_2 \rightarrow HD+D$ reaction: Comparison between experiment and theoretical predictions

Félix Fernández-Alonso[a)]
Istituto di Struttura della Materia, Consiglio Nazionale delle Ricerche, via del Fosso del Cavaliere 100, 00133 Rome, Italy

Brian D. Bean[b)] and Richard N. Zare
Department of Chemistry, Stanford University, Stanford, California 94305-5080

F. J. Aoiz, Luis Bañares, and Jesús F. Castillo
Departamento de Química Física, Facultad de Química, Universidad Complutense, 28040 Madrid, Spain

(Received 9 January 2001; accepted 18 June 2001)

We investigate the sensitivity of photoinitiated experiments to forward-scattering features by direct comparison of experimental angular distributions with quantum-mechanical calculations as well as by forward-convolution of theoretical and model center-of-mass differential cross sections. We find that the experimental sensitivity to forward-scattering angles depends on the instrumental velocity resolution as well as on the kinematics of the detected product channel. Explicit comparison is made between experimental HD($v'=1,2;j'$) center-of-mass angular distributions at collision energies $\approx$1.6 eV (deduced from time-of-flight profiles using a single-laser, photolysis-probe approach) and quantum-mechanical calculations on the BKMP2 potential energy surface. The comparison takes into account the contributions from both slow and fast H atoms from the photolysis of HBr. We find that the contribution of the slow H atoms, which is the major source of experimental uncertainty, does not greatly affect the extraction of the angular distribution from the experimental time-of-flight profile for a specific HD(v',j') state. Except for HD($v'=1, j'=8$) and HD($v'=2, j'=0$), for which either slow H atoms or the presence of a narrow forward-scattering peak make the analysis more uncertain, the agreement between experiment and theoretical predictions is excellent.
 [DOI: 10.1063/1.1390505]

I. INTRODUCTION

The past few years have witnessed unprecedented experimental advances in the investigation of the $H+H_2$ reaction and its isotopic variants with the first reports of state-resolved angular distributions at well-defined collision energies.[1–12] Laser methods to photoinitiate the chemical reaction and to detect the minute product yields into specific product rovibrational states have made such a breakthrough possible.

One of these approaches, the so-called photoloc technique (*photo* initiated reaction analyzed via the *l*aw *o*f *c*osines),[13–15] uses laser photolysis with a well-defined electric-field polarization to initiate the chemical reaction in a coexpanded mixture of a photolytic precursor and reagent. A measurement of the product laboratory speed distribution for a particular rovibrational product state allows a determination of the corresponding center-of-mass angular distribution. Measurement of this laboratory speed distribution has been achieved by the use of multiphoton ionization detection of the reaction product coupled to velocity-sensitive time-of-flight mass spectrometry for a number of chemical reactions including $H+D_2$,[1–4,11] $Cl+HD$,[16] $Cl+CH_4$,[17,18] and $Cl+C_2H_6$.[19–21]

The photoloc technique permits a measurement of center-of-mass angular distributions over the entire scattering angular range with an experimental resolution comparable to more demanding crossed molecular beam techniques. Such a complete coverage from forward to backward scattering is not generally possible in crossed-molecular-beam approaches where the laboratory-to-center-of-mass transformation combined with geometrical constraints introduced by the beam sources often mask portions of the product center-of-mass angular distribution. In the very elegant and elaborate crossed-beam experiments on the $H+D_2$ reaction carried out by Schnieder, Welge, and co-workers,[5–10,12] the experimental design of the apparatus leads to a complete insensitivity to product scattering below 50° (these laboratory angles are buried in the D_2 beam). Despite the very high quality of the data obtained by this group, their technique has been unable to measure a potentially very interesting scattering region, which is sensitive to the very details of the dynamics of this reaction system. As we show in this work, such a limitation is not generally present in the photoloc approach.

Using the photoloc technique, Zare and co-workers have recently reported experimental center-of-mass angular distributions for HD($v'=1, j'$) (Ref. 3) and HD($v'=2, j'$) (Ref. 4) product states at collision energies $\approx$1.6 eV. The authors measured core-extracted time-of-flight profiles with a one-

a)Author to whom correspondence should be addressed. Electronic mail: felix@ism.rm.cnr.it
b)Present address: Department of Chemistry, Pomona College, Claremont, California 91711.

laser experimental geometry. In this approach, the same laser pulse was utilized to photolyze the HBr precursor and to detect the nascent HD(v', j') laboratory speed. A carefully calibrated velocity basis set was employed to invert the experimental signals into the corresponding center-of-mass angular distributions. The well-justified assumptions are made that the slow HBr photolysis channel does not contribute more than 10%–15% to the measured signal and the experimental velocity resolution is sufficient to justify the uniqueness of the speed-to-scattering-angle inversion procedure. These experimental results showed a clear dependence of the angular distributions on product rotational quantum number and were consistent with a hard-sphere reaction model where the initial impact parameter is preferentially channeled into product rotation. No theoretical calculations, however, were available at the time for a direct comparison with the experimental data.

As a continuation of this line of work on the $H+D_2$ exchange reaction, we report a detailed comparison between experiment and quantum mechanical (QM) calculation on the Boothroyd, Keogh, Martin, and Peterson[22] (BKMP2) potential energy surface. This PES has proved to be one of the most accurate up to date.[6] We have taken special care to examine the effect of the slow HBr photolysis channel as well as the adequacy of the inversion procedure used to obtain center-of-mass angular distributions from the experimental raw data. The quantitative agreement between theory and experiment that we report in Sec. III B 1 supports the validity of our original assumptions (which were made prior to the availability of QM results) and suggests that the photoloc technique is well-suited for the study of this important reaction system. However, the lower sensitivity to the forward region, especially to very sharp scattering features, calls for a closer interplay of experiment and theory. In particular, we find that for the state HD($v'=2, j'=0$) the raw experimental data is consistent with the theoretical results but the inversion of the experimental velocity distribution is not capable of providing the fine details of the scattering process at very small angles. Strong forward-scattering features for $H+D_2 \rightarrow HD(v'=3, j'=0)+D$ at 1.64 eV have been recently observed by Zare and co-workers[1] using a two-laser, photolysis-probe approach. Reduced-dimensionality QM calculations by Truhlar and co-workers[23] have shown a correspondence between these experimental findings and a scattering resonance for the compound state HDD($v_1=3$, $v_2=0, J=20$). Such a study constitutes the first experimental observation of resonance behavior in the state-resolved differential cross section for the $H+D_2$ reaction system. In light of these new findings and the increasing availability of well-converged QM differential cross sections over a fine grid of collision energies,[24–26] we pay special attention in Secs. III B 2 and III C to analyzing our present experimental sensitivity to the forward-scattering region. Our intent is to provide the proper framework for a full exploitation of the experimental data obtained using the photoloc technique.

II. METHODS

A. Experiment

The experimental implementation of the photoloc technique for the $H+D_2 \rightarrow HD(v', j')+D$ reaction system has been described in detail in previous publications.[2–4] We limit ourselves to provide a brief account relevant to the present comparison with theoretical calculations.

A 1:4 mixture of HBr and D_2 is expanded into a vacuum chamber by means of a pulsed nozzle valve. A single, linearly polarized laser pulse operating in the range of 208–218 nm is used to photolyze the HBr precursor and to detect simultaneously and state-selectively the nascent HD(v', j') reaction product by (2+1) resonance-enhanced multiphoton ionization (REMPI) through the *Q*-branch members of the HD EF $^1\Sigma_g^+ - X\,^1\Sigma_g^+(0, v''=1,2)$ bands. As previously shown,[27] this detection scheme is most sensitive (i.e., within a few percent) to the number density of the probed molecules. Single-collision conditions were ensured by performing the experiments 25–35 nozzle diameters away from the beam source. With this experimental approach, we only collect those HD molecules generated during the duration of the laser pulse, whose temporal width lies between 5 and 6 ns. The collision energy resolution of these experiments is ≈50 meV full width at half maximum (FWHM) and it mainly arises from the residual translational temperature of our beam expansion ($T \sim 50$ K). Such a spread in collision energy is of a similar magnitude to the variations in collision energy caused by the scanning of the photolysis-probe laser across different HD(v', j') REMPI resonances. The D_2 reagent internal energy distribution has been characterized by (2+1) REMPI and corresponds to 0.45:0.35:0.10 in the $j''=0, 1, 2$ levels of the ground vibrational level ($T_{rot} \sim 90$ K). HBr photolysis in our wavelength range generates fast and slow H atoms correlating with Br($^2P_{3/2}$) and Br($^2P_{1/2}$), respectively.[28–30] Branching fraction measurements in our laboratory[2] and in others[30] show that the slow photolysis channel has a photolysis branching fraction of ≈0.15 at the photolysis wavelengths of the experiments.

After HBr photolysis and subsequent HD ionization, product ions travel inside a Wiley–McLaren time-of-flight spectrometer. A core extractor (3 mm radius) placed along the time-of-flight axis selects only those ions with maximal speed projections along the time-of-flight (detection) axis prior to their detection by a microchannel plate detector. In all the experiments, the photolysis-probe laser polarization was perpendicular to the detection axis. To avoid space-charge effects and other experimental artifacts, all the experiments were conducted under single-ion-counting conditions with typical collection times ranging between 1.5×10^3 and 3×10^3 laser shots at a 10 Hz repetition rate. The core-extracted time-of-flight profiles are digitized and stored in a personal computer for inversion of the laboratory speed distribution into center-of-mass angular distributions.

B. Theory

All the theoretical calculations have been carried out on the BKMP2 PES.[22] The QM reactive scattering calculations for the $H+D_2(v=0, j=0)$ reaction have been performed us-

TABLE I. Summary of experimental and theoretical parameters.

	Collision energy (eV)				HBr photolysis		
	Experiment		QM calculation		Branching fraction	Spatial anisotropy β	
HD(v', j')	Fast	Slow	Fast	Slow	Br*/(Br+Br*)	Fast	Slow
(1,1)	1.71	1.37	1.70	1.39	0.15	−1.0	1.0
(1,5)	1.70	1.34	1.70	1.30	0.15	−1.0	1.0
(1,8)	1.66	1.30	1.64	1.30	0.15	−1.0	1.0
(2,0)	1.56	1.20	1.55	1.20	0.15	−1.0	1.2
(2,3)	1.55	1.19	1.55	1.20	0.15	−1.0	1.2
(2,5)	1.53	1.17	1.55	1.15	0.15	−1.0	1.2

ing a coupled-channel hyperspherical coordinate method[31] at a total of 7 collision energies in the range 1.15–1.70 eV. The precise values of the collision energies employed in the calculations are shown in Table I. They closely correspond to the experimental values to ensure a meaningful comparison. At these collision energies, well-converged integral and differential cross sections have been obtained by using the parameters $j_{max}=17$, $E_{max}=2.65$ eV, and $k_{max}=11$ and by including all partial waves up to total angular momentum $J=34$. Further computational details have been given in previous work on this reaction system.[5] For comparison purposes, we have also carried out quasiclassical trajectory (QCT) calculations. Batches of 2×10^6 trajectories were run at 1.55 and 1.70 eV collision energies and a batch of 4×10^6 trajectories was run at 1.64 eV. The details of the QCT method employed for the present calculations have been described elsewhere.[6,32]

III. RESULTS AND DISCUSSION

Table I provides a summary of the experimental and theoretical parameters used in the present work. The experimental results may be subdivided into two groups, namely, HD($v'=1, j'$) at collision energies centered around 1.70 eV, and HD($v'=2, j'$) at 1.55 eV. The present QM calculations performed in the collision energy range 1.15–1.70 eV allow for a comparison with experimental results well within the experimental collision energy resolution of 50 meV. We also list in Table I the experimentally determined HBr photolysis branching fractions as well as the spatial anisotropies at the collision energies of our experiments. We note that while the fast H-atom spatial anisotropy remains constant over our photolysis wavelength range, the slow channel anisotropy depends more steeply on the wavelength. Over our range of photolysis wavelengths, $\beta_{slow}\approx1.0$ for HD($v'=1, j'$) and $\beta_{slow}\approx1.2$ for HD($v'=2, j'$),[30,33] which indicates the increasing contribution of perpendicular character for this photodissociation channel with respect to the purely parallel behavior ($\beta=2.0$) observed closer to the energetic threshold.[29,30,33] This information is necessary to carry out a detailed comparison with theory at the level of angular distributions and forward-convoluted time-of-flight profiles (Sec. III B).

A. Theoretical results

To initiate our discussion on forward-scattering features in the $H+D_2$ reaction, we show in Fig. 1 the theoretical QM and QCT differential cross sections for the product states relevant to this work as a function of center-of-mass scattering angle θ_r. Both QM and QCT angular distributions follow very similar trends, and the agreement between both sets of calculations is in some cases very good, as it has been shown previously at other collision energies.[5,6,10] Such a nearly quantitative agreement is not only true for the absolute value of the differential cross section but also for finer details of the angular distributions (most probable value, width, dependence on product rotational level, etc.).

Despite this overall good agreement between QM and QCT differential cross sections, the QCT calculations tend to smooth out the oscillatory behavior of the QM differential cross sections and to underestimate the amount of forward scattering by as much as a factor of 4 for HD($v'=2, j'=0$). We also note that forward scattering is most prominent for the states with the largest (smallest) amount of vibrational (rotational) excitation.

B. Comparison between experiment and QM predictions

1. Differential reaction rates

In order to incorporate the contribution of both photolysis channels in the theoretical predictions, we need to bear in mind that the experiment is only sensitive to the total number density of reaction products generated within the temporal envelope of the photolysis-probe laser. Typically, the rate of HD(v', j') product formation is given by the familiar expression,

$$\frac{dn_{HD}}{dt}=(n_H\cdot n_{D_2})\cdot\left(\sum_i k_i(E_{coll})\cdot X_i\right), \tag{1}$$

where n_H and n_{D_2} are the total number densities of the reactants, $k_i(E_{coll})$ is the reaction rate for reaction into a given HD(v', j') state at a collision energy E_{coll}, and X_i is the branching fraction for the ith photolysis channel. In our particular case, the sum in Eq. (1) reduces to two terms with $X_i=0.85$ and 0.15, corresponding to the fast and slow HBr photolysis channels, respectively. The reaction rate $k_i(E_{coll})$ is given by

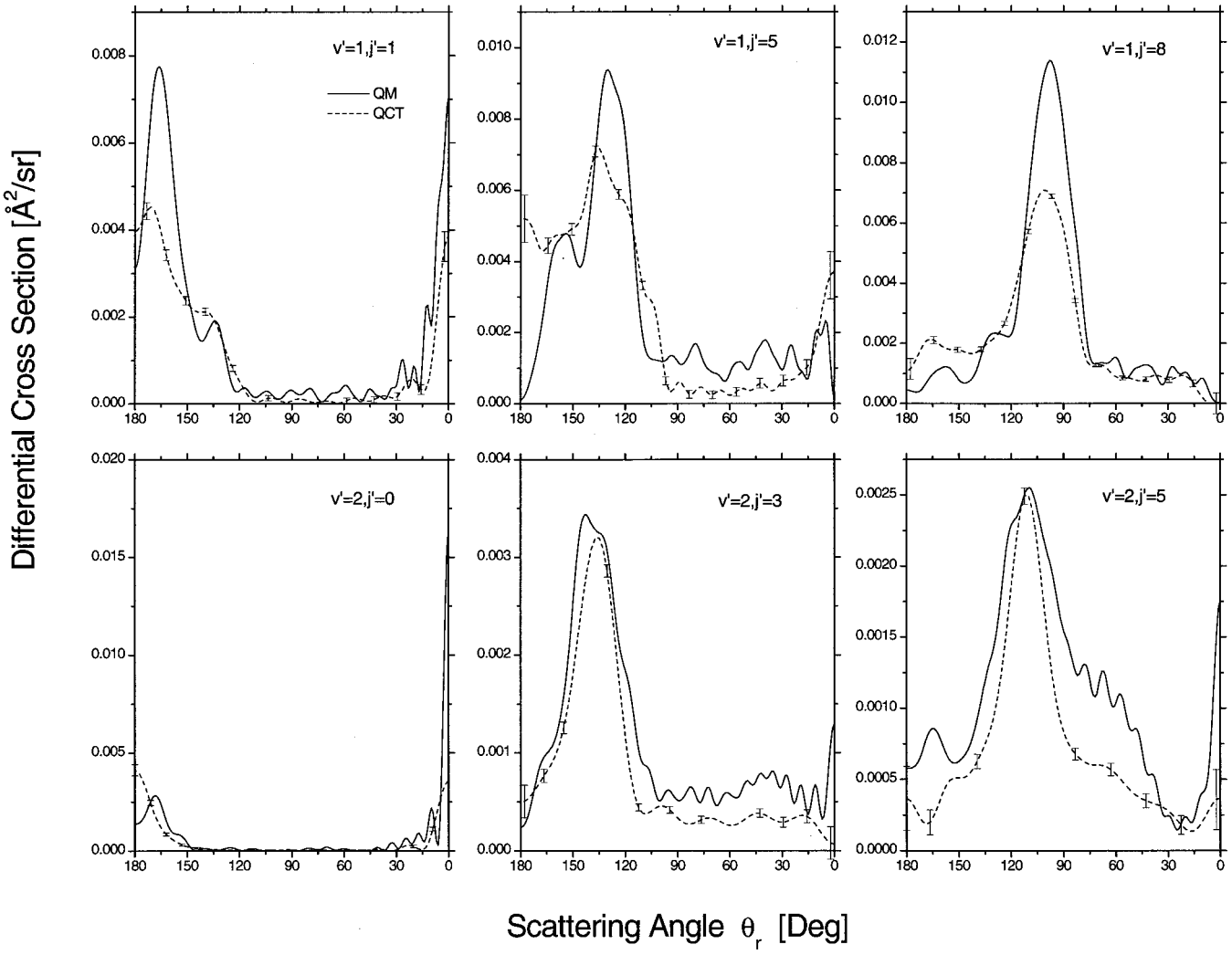

FIG. 1. QM and QCT differential cross sections for all the HD(v',j') product states relevant to this work. The collision energies of the calculated differential cross sections correspond to those of the fast HBr photolysis channel (see Table I). Error bars in the QCT angular distributions correspond to $1-\sigma$.

$$k_i(E_{\text{coll}}) = \sigma_i(E_{\text{coll}}) \cdot \nu_i , \tag{2}$$

where $\sigma_i(E_{\text{coll}})$ is the reaction cross section and $\nu_i = \sqrt{2E_{\text{coll}}/\mu_{\text{H-D}_2}}$ is the relative speed of the collision pair for the ith photolysis channel. Within the first few nanoseconds there is a negligible depletion of the reactant number densities ($n_{\text{H}}, n_{\text{D}_2} \gg n_{\text{HD}}$). Consequently, the total number of HD products n_{HD} detected in the experiments is given by time integration of Eq. (1) taking into account the temporal line shape of the excitation-detection laser (see Appendix). The result can be written as

$$n_{\text{HD}} = (n_{\text{H}} \cdot n_{\text{D}_2}) \cdot \left(\sum_i k_i(E_{\text{coll}}) \cdot X_i \right) \cdot \int_0^{+\infty} g_{\text{phot-probe}}(t)\, dt, \tag{3}$$

where $g_{\text{phot-probe}}(t)$ is a function that depends on the temporal profile of the laser as well as on the specifics of the absorption and detection steps. This last term in Eq. (3) is identical for both photolysis channels. Therefore, it does not need to be explicitly considered in the present comparison. The last term amounts to a numerical constant that depends only on the specifics of the experimental procedure, i.e., it merely represents the absolute number of HD products detected. Consequently, we can define a solid-angle differential product yield and differential reaction rate as

$$\frac{\partial n_{\text{HD}}}{\partial \Omega_r} = (n_{\text{H}} \cdot n_{\text{D}_2}) \cdot \left(\sum_i \frac{\partial k_i(E_{\text{coll}})}{\partial \Omega_r} \cdot X_i \right) \cdot \int_0^{+\infty} g_{\text{phot-probe}}(t)\, dt, \tag{4}$$

where the differential reaction rate $\partial k_i(E_{\text{coll}})/\partial \Omega_r$ is related to the calculated differential cross section $\partial \sigma_i(E_{\text{coll}})/\partial \Omega_r$ by an analogous expression as that shown by Eq. (2),

$$\frac{\partial k_i(E_{\text{coll}})}{\partial \Omega_r} = \frac{\partial \sigma_i(E_{\text{coll}})}{\partial \Omega_r} \cdot \nu_i . \tag{5}$$

Therefore, for a comparison of specific HD(v',j') product

states it is only necessary to know the corresponding differential reaction rates and branching fractions for the fast and slow HBr photolysis channels.

To account for the effects of instrumental resolution in the present comparison, we have blurred the theoretical distributions by the instrument function. In previous work,[2] calibration of the instrument with single-speed velocity distributions has showed that the experimental resolution in velocity space (i.e., time-of-flight profile) may be approximately modeled by the use of a Gaussian line shape, i.e.,

$$f_{\text{inst}}(\nu-\nu_i)=\left(\frac{1}{\delta_\nu\sqrt{\pi}}\right)\cdot e^{-((\nu-\nu_i)/\delta_\nu)^2}, \tag{6}$$

where δ_ν is related to the FWHM of the instrument function by $\delta_\nu=\text{FWHM}/2\sqrt{\ln 2}$. The value for δ_ν is directly obtained from the total laboratory speed range and the number of basis functions employed in the inversion of experimental time-of-flight profiles. We note that the instrumental resolution δ_ν is constant in velocity space, but not when expressed in terms of the variable $\cos\theta_r$. Such an angle-dependent resolution is a direct consequence of the nonlinear mapping between product laboratory speed ν_{HD} and center-of-mass scattering angle θ_r given by the law of cosines,

$$\nu_{\text{HD}}^2=u_{\text{CM}}^2+u_{\text{HD}}^2+2\cdot u_{\text{CM}}\cdot u_{\text{HD}}\cdot\cos\theta_r, \tag{7}$$

where u_{CM} is the center-of-mass speed and u_{HD} is the product speed in the center-of-mass scattering frame. From Eq. (7), we find that the approximate angular resolution $\delta_{\cos\theta_r}$ is related to the (constant) experimental time-of-flight resolution δ_ν by

$$\delta_{\cos\theta_r}=\left(\frac{\nu_{\text{HD}}}{u_{\text{CM}}\cdot u_{\text{HD}}}\right)\cdot\delta_\nu. \tag{8}$$

From previous work on this reaction system,[2–4] the resulting angular resolution in the experimental data varies from 5° to 6° in the backward ($\cos\theta_r=-1$) to 12°–13° in the forward scattering region ($\cos\theta_r=+1$).

The angle-dependent instrumental function required to blur the theoretical angular distributions may be obtained from Eq. (6) as follows:

$$\begin{aligned} f_{\text{inst}}(\cos\theta_r-\cos\theta_{r,i}) &= f_{\text{inst}}(\nu-\nu_i)\cdot\left(\frac{d\nu}{d\cos\theta_r}\right) \\ &= f_{\text{inst}}(\nu-\nu_i)\cdot\left(\frac{u_{\text{CM}}\cdot u_{\text{HD}}}{\nu}\right). \end{aligned} \tag{9}$$

Finally, the blurred angular distribution is given by convolution of Eq. (9) with the theoretical angular distribution,

$$\left\langle\frac{\partial k}{\partial\Omega_r}\right\rangle_{\cos\theta_{r,i}}=\int_{-1}^{+1}\left(f_{\text{inst}}(\cos\theta_r-\cos\theta_{r,i})\cdot\left(\frac{\partial k}{\partial\Omega_r}\right)_{\cos\theta_r}\right)d\cos\theta_r. \tag{10}$$

Figure 2 shows a comparison of the experimental and blurred theoretical angular distributions. We have included in each plot the contributions of both photolysis channels weighted by their occurence (cf. Table I). The experimental points have been obtained from linear least-squares fits using evenly spaced velocity basis functions as described in detail previously.[2,33] The experimental angular distributions have been scaled to the same area as the corresponding theoretical distributions. Their associated error bars represent $1-\sigma$ uncertainty bands. The effect of the instrument function on the theoretical distributions is not major in the backscattering hemisphere but it clearly broadens and flattens the sharp forward-scattering peaks of the low-j' states. Overall, the agreement between experimental and theoretical predictions is very satisfactory. For both HD($v'=1,j'$) and HD($v'=2,j'$) reaction products, the angular distributions shift from backward toward sideways scattering as the product rotational angular quantum number increases. Qualitatively, this behavior is the expected dependence of a direct reaction where the initial impact parameter (initial orbital angular momentum) is preferentially channeled into product rotation.[3,4]

The contribution of the slow photolysis channel to the total differential reaction rate is greatest for HD($v'=1,j'=1$) product state (19.5%) for which the state-specific total reaction cross section at the lower collision energy of 1.39 eV is ~1.3 times greater than the corresponding one at 1.70 eV. The shape of the angular distribution, however, is not greatly modified by the incorporation of the slower reaction channel and the agreement with experiment remains very satisfactory. The smallest contribution of the slow channel (0.02%) occurs for HD($v'=2,j'=5$). All other rovibrational product states fall between these two limits with an average contribution of the slow channel of ~11%. This value is within our previous estimates ranging 10%–15%,[3,4] which justified the inversion of the experimental data into center-of-mass angular distributions prior to the availability of theoretical calculations. It is expected, however, that neglect of the slow reaction channel will make the agreement for the finest details of the angular distribution less quantitative. The QM calculations shown in Figs. 1 and 2 have only been performed for the rotationless state of the D_2 reagent while, as explained in Sec. II A, our experimental diatomic reagent distribution spreads over the first three rotational levels. Whereas we have not incorporated all rotational levels in our comparison we expect that differences with the presented results will be minor. This claim is substantiated by quasiclassical trajectory calculations at 1.29 eV by Aoiz *et al.*[34] as well as the very satisfactory agreement between theory and experiment evidenced by the results shown in Fig. 2.

The agreement between experiment and calculation at the level of angular distributions is less satisfactory in two situations. For the HD($v'=1,j'=8$) state, the contribution of the slow channel to the total differential reaction rate is well within the experimental error bars reported (cf. Fig. 2). There is, nevertheless, a sensible discrepancy between experimental and theoretical distributions in the backscattering region, the experimental distribution being broader than the theoretical one. In addition, the calculated HD($v'=2,j'=0$) shows an intense and narrow forward scattering peak not present in the experimental angular distributions. A similar but less dramatic forward-scattering peak is also present

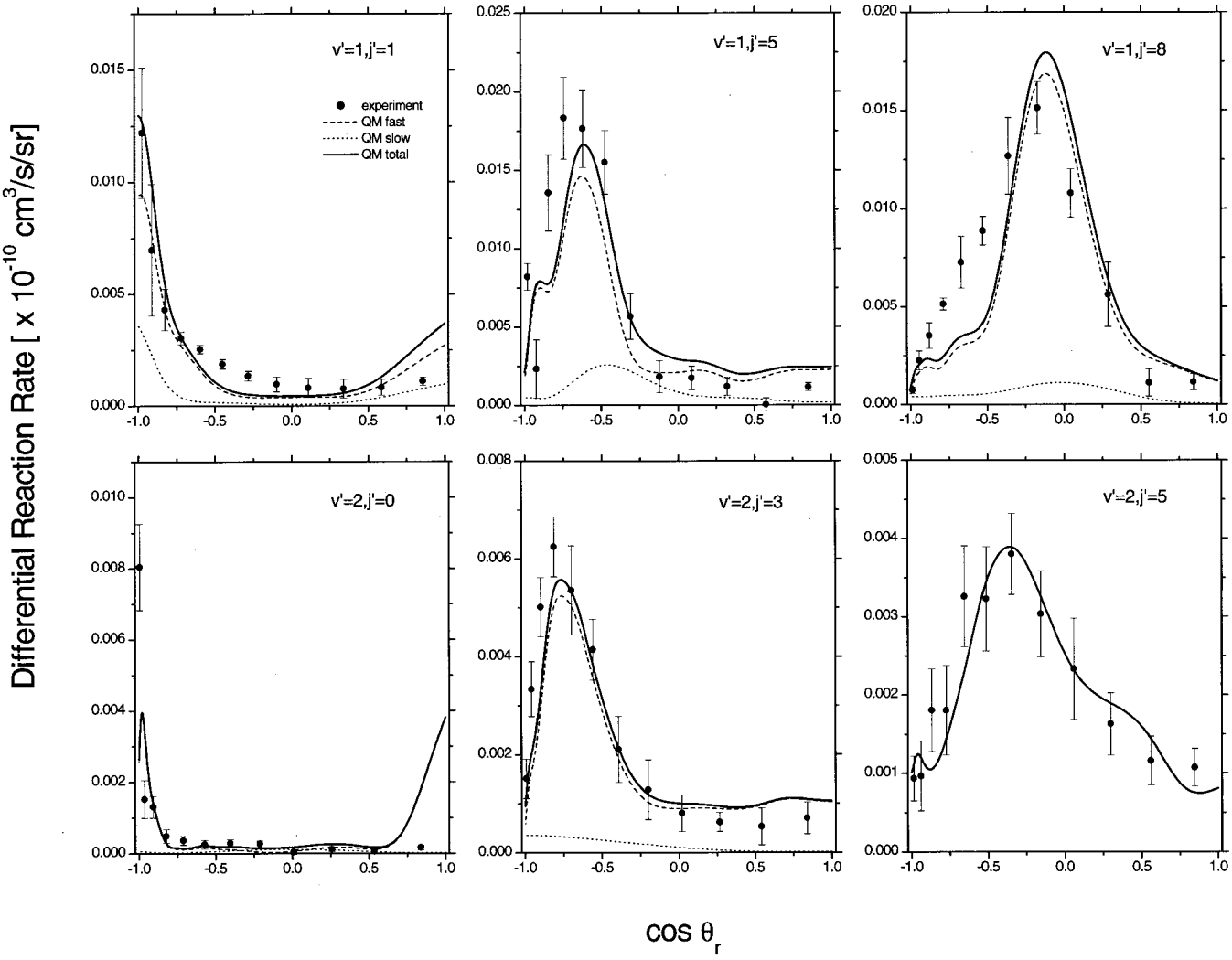

FIG. 2. Comparison of experimental and blurred theoretical angular distributions for all the HD(v',j') relevant to this work. Dashed and dotted lines correspond to the contributions of the fast and slow HBr photolysis channel, respectively. The experimental points (filled circles) are shown along with their associated $1-\sigma$ error bars. Table I shows the experimental and theoretical collision energies used for each HD rovibrational state.

for HD($v'=1, j'=1$). We note, however, that the experimental data for this state was obtained at lower resolution and, thus, we expect to be less sensitive to the less-pronounced forward scattering peak. As mentioned before and discussed in previous publications,[2–4] the angular resolution of photoloc experiments is angle-dependent, being best in the backward-scattering region and worst in the forward-scattering region. In spite of this decrease in forward scattering resolution, it should still be possible to obtain meaningful information about the fastest moving products. In order to extract such information, it is necessary to complement the speed-to-angle inversion procedure with a more direct approach. Thus, we were motivated to investigate a forward-convolution of the theoretical angular distributions into time-of-flight profiles to allow for a direct comparison of the theoretical predictions with the raw experimental data.

2. Forward-convoluted time-of-flight profiles

In Sec. III B 1 we compared experiment and theory at the level of angular distributions. While a theoretical approach calculates directly the differential cross section, the experimental data has been obtained from an inversion of the laboratory product velocity distribution (time-of-flight profile) into an angular distribution. A necessary step in such a procedure is to define a finite product laboratory velocity basis set and to perform a linear least-squares fit of the experimental signal. The size of this basis set (number of basis functions) is determined by the instrumental velocity resolution and it has been obtained by an extensive calibration of the instrument using single-speed velocity distributions arising from photolysis and chemical reaction.[2,33] Implicit in this analysis is the assumption that there is sufficient instrumental resolution to obtain a nearly unique fit of the experimental signal.

The comparison presented in the previous section between experiment and theory corroborates to a great extent the adequacy of this approach. Nevertheless, it is still possible to test further the method by calculating the time-of-flight profiles that would result from the theoretical angular distributions and to compare them with the raw experimental data. To this end, we proceeded as follows. In our photoloc

experiment, the center-of-mass angular distribution from chemical reaction for a particular HD(v',j') quantum state is related to the three-dimensional laboratory velocity distribution by the following expression:[13]

$$P(\underline{v}_{\mathrm{HD}}) = \left(\frac{1}{2\cdot u_{\mathrm{CM}}\cdot u_{\mathrm{HD}}\cdot v_{\mathrm{HD}}}\right)\cdot\left(\frac{1}{\sigma}\frac{d\sigma}{d\Omega_r}\right) \cdot[1+\beta_{\mathrm{rxn}}(\hat{u}_{\mathrm{CM}}\cdot\hat{v}_{\mathrm{HD}})\cdot P_2(\hat{\epsilon}_{\mathrm{phot}}\cdot\hat{v}_{\mathrm{HD}})], \tag{11}$$

where u_{CM}, u_{HD}, v_{HD} retain the same meaning as before, the superscript carats denote unit vectors, and $\hat{\epsilon}_{\mathrm{phot}}$ corresponds to a unit vector along the photolysis laser polarization. The second term in Eq. (11) corresponds to the normalized differential cross section at a given solid angle. To include the effects of both photolysis channels in this simulation, it is only necessary to replace this second term by the corresponding differential reaction rate and to sum over all possible photolysis channels taking into account their different photolysis anisotropies (see Table I).

Using the same instrumental parameters as those employed in the analysis of the experimental data, we have performed a Monte Carlo simulation of the theoretical angular distributions. Briefly, the simulation is performed by sampling the three-dimensional velocity distribution shown in Eq. (11). The probability of an ion packet with a definite laboratory speed and angular anisotropy is computed for a given experimental geometry taking into account the instrumental velocity resolution. The parametrizations used to describe the instrument function have already been described in detail in previous work.[2,33]

The resulting forward-convoluted, core-extracted time-of-flight profiles are shown in Figs. 3 and 4 for all the product rovibrational states. We also show the contributions of the two photolysis channels to the total forward-convoluted time-of-flight profile in an analogous manner to what was shown in Fig. 2. As before, we have normalized the experimental and theoretical time-of-flight profiles to the same area for ease of comparison.

The slower photolysis channel has a more visible effect for the HD($v'=1,j'$) states with contributions ranging from ≈20% for HD($v'=1,j'=1$) and HD($v'=1,j'=5$) to 15% for HD($v'=1,j'=8$). For HD($v'=1,j'=1$) and HD($v'=1,j'=5$) the overall shape of the forward-convoluted time-of-flight profile does not change appreciably after the inclusion of the slower channel. Specifically, for HD($v'=1,j'=5$), the slight lower weight given to the slow-moving signal can account for the minor differences between theory and experiment in the position of the backscattering local minimum. A more interesting scenario is revealed for HD($v'=1,j'=8$). In this case, the time-of-flight profile has shifted to higher product laboratory speeds (more sideways scattering) for both photolysis channels (cf. Figs. 1 and 2). However, the slow photolysis channel has a noticeably narrower velocity span and the resulting time-of-flight profile falls in a range corresponding to backward scattering for the fast photolysis channel. Because the experimental sensitivity after core-extraction is largest for back-scattered products, addition of a mere 15% of signal to the slow portion of the time-of-flight results in an overestimation of the amount of backscattered product, consistent with the experimental angular distribution that assumed a single photolysis channel. From these considerations we conclude that it is quite justifiable to neglect the effect of the slow photolysis channel provided its contribution is small (10%–20%) and the prod-

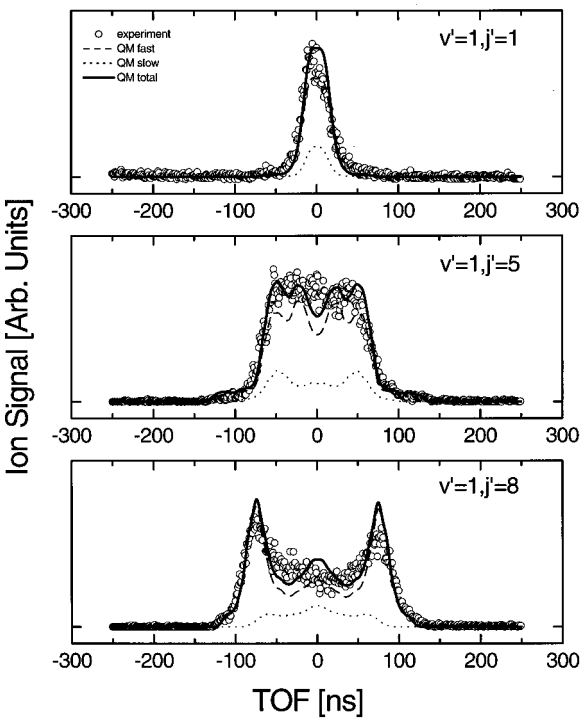

FIG. 3. Comparison between experimental HD($v'=1,j'$) time-of-flight profiles and the corresponding forward convolutions of the QM angular distributions. As in Fig. 2, we show the contributions of the two HBr photolysis channels to the total signal (see legend in the figure).

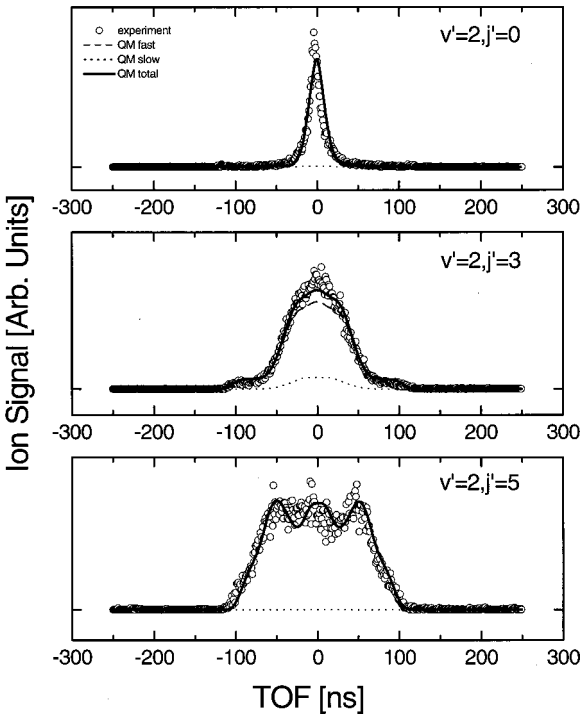

FIG. 4. Same as Fig. 3 but for HD($v'=2,j'$) product states.

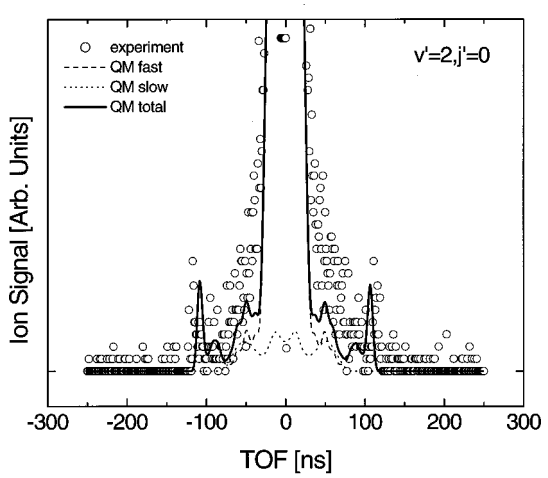

FIG. 5. Blow-up of the experimental time-of-flight profile and theoretical forward convolution corresponding to HD($v'=2, j'=0$). In both experiment and calculation, there is a clear contribution of the fastest moving HD products. This signature corresponds to the forward-scattering peak shown in Figs. 1 and 2 for this product state.

uct laboratory speed ranges are similar, i.e., both channels are away from the energetic reaction threshold and their collision energies are not very dissimilar.

For the HD($v'=2, j'$) states (see Fig. 4), the contribution of the slow photolysis channel to the time-of-flight profile has decreased considerably with respect to HD($v'=1, j'$). The worst case is HD($v'=2, j'=3$) with a 9% contribution which does not greatly modify the shape of the forward-convoluted time-of-flight profile. For HD($v'=2, j'=0$) and HD($v'=2, j'=5$) the slow-channel contribution has decreased to 3% and 0.04%, respectively. The agreement between the simulated and experimental time-of-flight profiles is excellent. Such an agreement is also present in the angular distributions, specially for HD($v'=2, j'=3$) and HD($v'=2, j'=5$). For HD($v'=2, j'=0$), the time-of-flight profiles show a narrow back-scattered (slow) peak both in the theoretical forward-convoluted and experimental profiles, consistent with predominant backscattering. The narrow yet intense forward scattering feature in the calculated angular distribution (see Fig. 1) appears as two very weak peaks at the maximal product laboratory speed. In Fig. 5 we show an enlarged view of the HD($v'=2, j'=0$) time-of-flight profiles. The experimental time-of-flight profile is consistent with the two narrow fast-moving peaks corresponding to the forward-scattering signature (cf. Figs. 1 and 2). Also note that over these product laboratory speeds the slow channel does not contribute and, therefore, all the signal experimentally observed at these laboratory speeds corresponds to fast (forward-scattered) HD($v'=2, j'=0$) product arising from the fast channel. Nevertheless, the total amount of signal corresponding to forward scattering is very small. We estimate that for this product state only a few ions out of 300–400 ions at the peak of the profile were detected in the course of the experimental runs, thereby giving rise to the large amount of shot noise in the experimental profile. In velocity space, the width of this forward-scattering peak is on the order of 6 m/s compared to ≈1000 m/s for the backscattered peak. The total product laboratory velocity range is 7700 m/s. Moreover, we also need to incorporate the decreased sensitivity of the core-extraction technique to fast-moving products, which becomes particularly strong for certain product speed combinations (see Sec. III C). It is then understandable that an inversion procedure using a finite basis set with the lowest resolution in the forward-scattering region may not be capable of accounting for such a sharp and narrow scattering feature. Note that in Fig. 2 there is only one velocity basis function encompassing the angles for most forward scattering. Moreover, the least-squares fitting procedure used to extract the experimental angular distribution only tries to minimize the global chi-squares and is not very sensitive to small changes in the chi-squares induced by a better fit of the fast (forward-scattering) wings of the time-of-flight profile. We are then led to conclude that a detailed analysis of sharp, forward-scattering features in photoloc-derived angular distributions requires not only an inversion of laboratory time-of-flights into angular distributions using a finite laboratory velocity basis set but also a comparison of the experimental time-of-flights with forward-convoluted theoretical or model angular distributions.

C. Sensitivity of the photoloc technique to forward scattering

As a prelude to a quantitative analysis that follows in this section, a few qualitative remarks are in order. It is relatively simple to understand why core-extracted time-of-flight profiles suffer from a decreased sensitivity to forward scattering. To appreciate this feature, we assume that the chemical reaction produces equal amounts of fast- and slow-moving products with identical spatial anisotropies. The corresponding one-dimensional projection of this velocity distribution would be the arithmetic sum of two profiles of identical shape but with different velocity spans, i.e., the fast-moving one being stretched by a factor of $\nu_{\text{fast}}/\nu_{\text{slow}}$ with respect to the slow-moving one. An immediate consequence of such an addition is the unavoidable pile-up of contributions from different speeds at the same time-of-flight and a reduction of the experimenter's ability to invert with confidence the time-of-flight profile into a center-of-mass angular distribution, given the practical existence of experimental noise and finite instrumental resolution. By use of a core extractor, only the edges of each individual speed contribution are detected and, therefore, the amount of overlap between different product speeds is dramatically decreased. However, we also lose the ability to relate directly the relative amounts of products at different speeds (only a careful calibration of the instrument function can recover this information). Qualitatively, for our previous example of a fast- and slow-moving velocity distribution, and assuming perfect core-extraction, the core-extracted signals for the fast- (forward) and slow-moving (backward) products would approximately scale as

$$\frac{S_{\text{fast}}}{S_{\text{slow}}} \approx \frac{\nu_{\text{slow}}}{\nu_{\text{fast}}}. \tag{12}$$

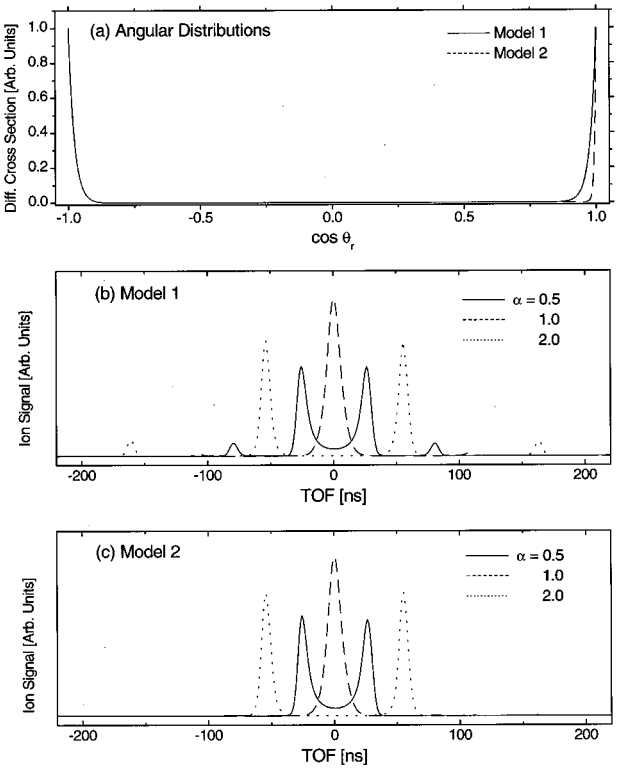

FIG. 6. Forward convolutions of forward-backward model angular distributions for several values of the α parameter (see text for definitions). (a) Model angular distributions. (b) and (c) Corresponding time-of-flight profiles.

From these simple considerations summarized by Eq. (12), it becomes apparent that for $\nu_{\text{fast}} \gg \nu_{\text{slow}}$, the experimental sensitivity to forward scattering approaches zero. Equation (11) may be used as a rough guide for the sensitivity to forward scattering of a given experiment. In practical situations, the limit $\nu_{\text{fast}} \gg \nu_{\text{slow}}$ is determined by both the instrumental resolution and the signal to noise ratio. More than an order-of-magnitude difference between the sensitivity to fast- and slow-moving products may be sufficient to add uncertainty to a direct inversion of the experimental data into a center-of-mass angular distribution, particularly in regard to the overall magnitude of forward-scattering peaks. In such a case, a direct forward-convolution procedure as the one described in Sec. III B 2 may be more appropriate.

To provide a more quantitative analysis of the sensitivity of photoloc experiments using core-extraction to forward-scattering features, we have carried out time-of-flight simulations of model forward–backward angular distributions closely resembling the situation existing for the HD($v'=2$, $j'=0$) product state. In Fig. 6(a) we show the model angular distributions used in these simulations. They correspond to Gaussian, forward–backward symmetric differential cross sections with angular widths of 10° half width at half maximum (HWHM) in the backward region and 10° and 5° HWHM in the forward region. We have employed the same simulation parameters as those used for the HD($v'=2, j'=0$) in Sec. III B 2 with the exception of the center-of-mass and laboratory product speeds, which we allowed to vary as explained below. The figure of merit in the forward-convoluted time-of-flight profiles shown in Figs. 6(b) and 6(c) is the parameter α, closely related to Eq. (12), and defined as[14]

$$\alpha = \frac{u_{\text{HD}}}{u_{\text{CM}}}. \tag{13}$$

This parameter is a direct measure of the feasibility of a photoloc experiment. The largest laboratory velocity range ν_{range} and, consequently, the largest number of single-speed velocity basis functions occurs when $\alpha=1$. This condition has been typically considered to be the optimal one for a photoloc experiment because it represents the point at which the experiment uses the largest range of product laboratory speeds resulting in a concomitant increase in the number of single-speed basis functions.[14] We see, however, that such is not the case in terms of the experimental sensitivity to forward scattering. In Figs. 6(b) and 6(c), the poorest sensitivity to forward scattering occurs for precisely this value of α. Such a lack of sensitivity is a consequence of the presence of a very strong $\nu_{\text{HD}} \approx 0$ peak in the time-of-flight profile arising from backward-scattered signal. For the other two cases ($\alpha=0.5$, 2.0), the situation is more favorable [cf. Fig. 6(b)] and the differences in sensitivity to forward and backward scattering remain within the same order of magnitude. Such an increase in sensitivity is, however, linked with a smaller range of laboratory speeds and, therefore, a smaller angular resolution.

For the state HD($v'=2, j'=0$), $\alpha=1.01$, a value approaching the worst case for forward-scattering sensitivity. This finding helps explaining the low experimental sensitivity to the theoretical forward-scattering peak, as evidenced by the inability of a global inversion procedure to grasp the rapidly varying feature at 0°. We also note the great sensitivity to the width of the forward peak. As shown in Figs. 6(b) and 6(c), a decrease of the forward scattered peak width by merely a factor of 2 completely alters our experimental sensitivity making the detection of a very narrow (5° or less) feature much more demanding for all values of α shown in the figure. A complete comparison of experimental and theoretical angular distributions requires full account of these considerations.

For the HD($v'=3, j'$) experimental angular distributions at $E_{\text{coll}}=1.64$ eV recently reported to exhibit a large forward-scattering component[1] the situation is closer to the case shown in Fig. 4(b) (α ranges between 0.3 and 0.7). Thus, our experimental sensitivity to forward scattering is enhanced with respect to the HD($v'=2, j'=0$) case presented in this work. This conclusion is confirmed by the lineshape of the experimental time-of-flight profiles, which show a noticeable fast component corresponding to the forward-scattering peak [see Fig. 6(b)]. Within the framework presented throughout this work, it should be possible to provide a direct comparison between theory and experiment in an attempt to understand the origin of resonance behavior in this reaction system manifested at the level of product-state-resolved angular distributions.

IV. CONCLUSIONS

The sensitivity of the photoloc technique to forward-scattering features has been thoroughly investigated by explicit comparison between one-laser experiments and QM predictions on the $H+D_2 \rightarrow HD+D$ exchange reaction. Overall, the agreement between experiment and theory is very satisfactory, illustrating the robustness of the inversion procedure typically used to extract dynamical information from photoloc experiments. Discrepancies between theory and experiment have been attributed to either the presence of the slower photolysis channel in the one-laser experiments, especially for $HD(v'=1, j'=8)$, and/or to the lower angular resolution and sensitivity in the forward scattering region for particular $HD(v', j')$ states. An alternative comparison between theory and experiment performed by explicit forward-convolution of the theoretical angular distributions corroborates the above conclusions. Furthermore, it shows that the forward-scattering peak present in the QM calculation for $HD(v'=2, j'=0)$ is consistent with the experimental raw data. Simulation of QM and model angular distributions show that care must be exercised in interpreting the exact form of forward-scattering features obtained from inversion of experimental time-of-flight data, i.e., the instrumental resolution and the kinematics of the detected $HD(v', j')$ state may broaden the sharpness of any forward-scattering feature. These simulations also demonstrate the significant gain in understanding that can be obtained when it is possible to forward-convolute reliable QM calculations for a comparison with raw experimental data.

ACKNOWLEDGMENTS

This work was supported at Stanford University by the U.S. National Science Foundation under Grant No. CHE-99-00305 and at Universidad Complutense by the Spanish CICYT under Grant No. PB98-0762-C03-01. F.F.A. acknowledges support in the form of a Marie Curie Fellowship of the European Program ''Improving Human Research Potential and the Socio-economic Knowledge Base'' under Contract No. HPMFCT-2000-00683. B.D.B. acknowledges Elf-Atochem for support in the form of a Graduate Fellowship. J.F.C. acknowledges financial support provided by the Program ''Acciones para la Incorporación de Doctores y Tecnólogos'' of the Spanish Ministry of Education, Culture, and Sport. The facilities provided by the Centro de Supercomputación Complutense (SG Origin 2000) are gratefully acknowledged.

APPENDIX: RATE EQUATION MODELING OF ONE-LASER EXPERIMENTS

The photolysis, chemical reaction, and product detection that takes place simultaneously under the temporal envelope of a single laser pulse may be written as

$$AX + h\nu \rightarrow A + X \quad \text{photolysis,} \tag{A1}$$

$$A + BC \rightarrow AB + C \quad \text{reaction,} \tag{A2}$$

$$AB + nh\nu \rightarrow AB^+ + e^- \quad \text{product detection,} \tag{A3}$$

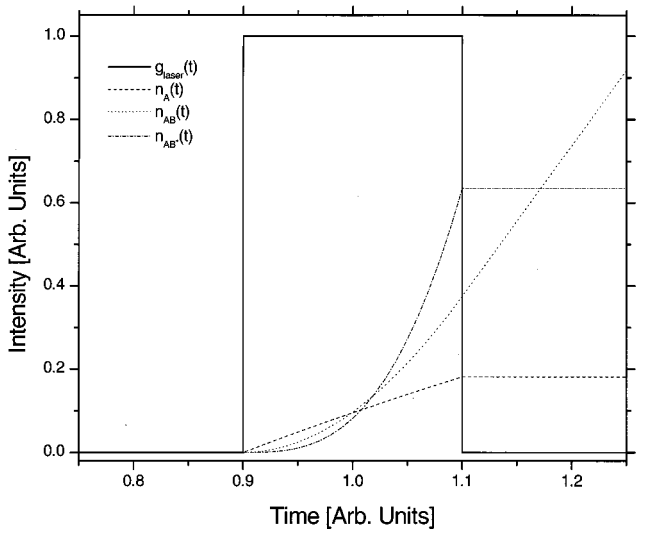

FIG. 7. Solution of the reactant and product temporal evolution upon excitation by a square laser pulse. The traces shown have been arbitrarily scaled to highlight their time dependence.

where AX is the photolytic precursor, A is the ''hot'' particle, BC is the molecular reagent, and AB and C are the reaction products. The system of first-order differential equations and initial conditions governing steps (A1)–(A3) is given by

$$\frac{dn_{AX}}{dt} = -k_{\text{phot}}(t) \cdot n_{AX} \quad n_{AX}(0) = n_{AX}^{\text{ini}}, \tag{A4}$$

$$\frac{dn_{BC}}{dt} = -k_{\text{rxn}} \cdot n_A \cdot n_{BC} \quad n_{BC}(0) = n_{BC}^{\text{ini}}, \tag{A5}$$

$$\frac{dn_A}{dt} = k_{\text{phot}}(t) \cdot n_{AX} - k_{\text{rxn}} \cdot n_A \cdot n_{BC} \quad n_A(0) = 0, \tag{A6}$$

$$\frac{dn_C}{dt} = k_{\text{rxn}} \cdot n_A \cdot n_{BC} \quad n_C(0) = 0, \tag{A7}$$

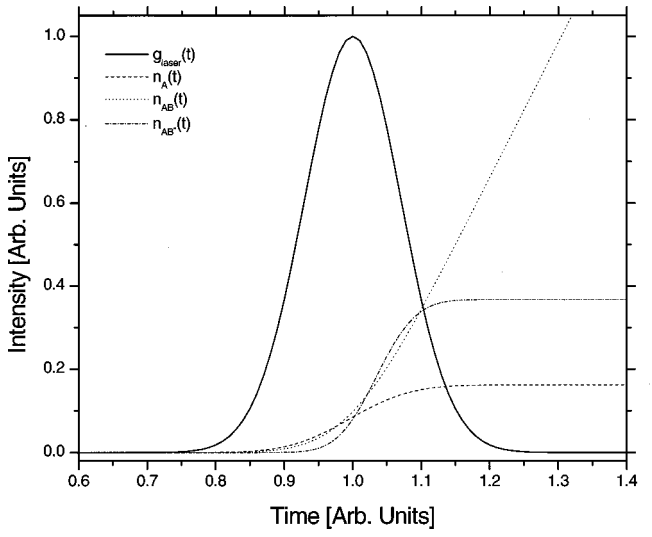

FIG. 8. Same as Fig. 7 but for a Gaussian laser pulse.

$$\frac{dn_{AB}}{dt} = k_{\mathrm{rxn}} \cdot n_A \cdot n_{BC} - k_{\mathrm{det}}(t) \cdot n_{AB} \quad n_{AB}(0) = 0, \tag{A8}$$

$$\frac{dn_{AB^+}}{dt} = k_{\mathrm{det}}(t) \cdot n_{AB} \quad n_{AB^+}(0) = 0, \tag{A9}$$

where $k_{\mathrm{phot}}(t)$, k_{rxn}, and $k_{\mathrm{det}}(t)$ are the photolysis, chemical reaction, and detection rates with units of s^{-1}, $cm^{-3}s^{-1}$, and s^{-1}, respectively. For the definition of k_{rxn}, the reader is referred to Eq. (2) in the main text. The time-dependent rate constants $k_{\mathrm{phot}}(t)$ and $k_{\mathrm{det}}(t)$ may be written as

$$k_{\mathrm{phot}}(t) = k_{\mathrm{phot}} \cdot g_{\mathrm{laser}}(t) = \sigma_{\mathrm{phot}} \cdot F \cdot g_{\mathrm{laser}}(t), \tag{A10}$$

$$k_{\mathrm{det}}(t) = k_{\mathrm{det}} \cdot g^n_{\mathrm{laser}}(t) = \sigma_{\mathrm{det}} \cdot (F \cdot g_{\mathrm{laser}}(t))^n. \tag{A11}$$

In Eq. (A10), σ_{phot} is the photolysis cross section (cm^2), F is the peak laser fluence (photons $cm^{-2}s^{-1}$), and $g_{\mathrm{laser}}(t)$ describes the temporal evolution of the laser pulse. All these quantities may be obtained experimentally for any given focusing geometry and photolytic precursor. Similar considerations also apply to Eq. (A11), where the effective detection cross section σ_{det} has units of $cm^{2n}s^{n-1}$. The use of Eqs. (A8), (A9), and (A11) to model the detection step deserves a few comments. In general, it is necessary to incorporate the presence of a resonant step and other decay channels of the excited state population AB^* that mediates the transition from the ground state AB neutral to the AB^+ ion. However, it is possible to show that to a first-order approximation, the total ionization rate for a $(n+m)$ resonant multiphoton ionization process follows a power law which scales as F^{n+m}.[35,36] Moreover, for the case of $(n+m)$ multiphoton ionization with $n>m$, the final ionization step tends to saturate first, approaching an F^n power dependence. Such power laws may be easily obtained by performing a laser intensity dependence of the ion signal. In our experiments using (2+1) REMPI, the power-law exponents typically vary between 2.0 and 3.0, indicating partial saturation of the ionization step.

Equations (A4)–(A9) can be solved numerically for any given laser temporal profile $g_{\mathrm{laser}}(t)$, photolysis, chemical reaction, and detection rates. However, the solution to this system of first-order differential equations can be greatly simplified after imposing two well-justified assumptions. Assume that the chemical reaction has a negligible contribution to the depletion of ''hot'' A atoms and BC molecules, i.e., over the duration of a nanosecond laser pulse, the first term in Eq. (A6) is typically 10^5-10^6 times greater than the second. Also assume that the detection step does not change appreciably the population of AB products, that is, it merely probes the product number density. With these two assumptions, the second terms on the right-hand side of Eqs. (A6) and (A8) may be set to zero. The solution to the time evolution of all species of interest is then given by successive time integration of the reagent, product, and ion populations,

$$n_{AX}(t) = n^{\mathrm{ini}}_{AX} \cdot e^{-\int_0^t k_{\mathrm{phot}}(u)du}, \tag{A12}$$

$$n_A(t) = n^{\mathrm{ini}}_{AX} \cdot \int_0^t k_{\mathrm{phot}}(u) \cdot e^{-\int k_{\mathrm{phot}}(u)du} du, \tag{A13}$$

$$n_{AB}(t) = k_{\mathrm{rxn}} \cdot n^{\mathrm{ini}}_{AX} \cdot n^{\mathrm{ini}}_{BC} \cdot \int_0^t \left(\int k_{\mathrm{phot}}(u) \cdot e^{-\int k_{\mathrm{phot}}(u)du} du \right) du, \tag{A14}$$

$$n_{AB^+}(t) = k_{\mathrm{rxn}} \cdot n^{\mathrm{ini}}_{AX} \cdot n^{\mathrm{ini}}_{BC} \cdot \int_0^t \left(k_{\mathrm{det}}(u) \cdot \int \left(\int k_{\mathrm{phot}}(u) \cdot e^{-\int k_{\mathrm{phot}}(u)du} du \right) du \right) du. \tag{A15}$$

Noting that the total number of ''hot'' A atoms produced by the laser pulse is given by

$$n^{\mathrm{total}}_A = n_A(\infty) = n^{\mathrm{ini}}_{AX} \cdot \int_0^\infty k_{\mathrm{phot}}(u) e^{-\int k_{\mathrm{phot}}(u)du} du, \tag{A16}$$

we can rewrite Eq. (A15) as

$$\begin{aligned} n_{AB^+}(t) &= k_{\mathrm{rxn}} \cdot n^{\mathrm{total}}_A \cdot n^{\mathrm{ini}}_{BC} \cdot \int_0^t \left(\frac{k_{\mathrm{det}}(u) \cdot \int (\int k_{\mathrm{phot}}(u) e^{-\int k_{\mathrm{phot}}(u)du} du) du}{\int_0^\infty k_{\mathrm{phot}}(u) e^{-\int k_{\mathrm{phot}}(u)du} du} \right) du \\ &= k_{\mathrm{rxn}} \cdot n^{\mathrm{total}}_A \cdot n^{\mathrm{ini}}_{BC} \cdot \int_0^t \left(\frac{\sigma_{\mathrm{det}} \cdot F^n \cdot g^n_{\mathrm{laser}}(u) \cdot \int (\int g_{\mathrm{laser}}(u) e^{-\int g_{\mathrm{laser}}(u)du} du) du}{\int_0^\infty g_{\mathrm{laser}}(u) e^{-\int g_{\mathrm{laser}}(u)du} du} \right) du. \end{aligned} \tag{A17}$$

After integration of Eq. (A17) from zero to infinity, it becomes identical in form to Eq. (3) in the text, that is, the integrand of Eq. (A17) corresponds to the function $g_{\mathrm{phot\text{-}probe}}(t)$. For illustration purposes we show in Figs. 7 and 8 the solutions for the case of square and Gaussian laser temporal profiles.

[1] F. Fernández-Alonso, B. D. Bean, J. D. Ayers, A. E. Pomerantz, R. N. Zare, L. Bañares, and F. J. Aoiz, Angew. Chem. Int. Ed. Engl. **39**, 2748 (2000).

[2] F. Fernández-Alonso, B. D. Bean, and R. N. Zare, J. Chem. Phys. **111**, 1022 (1999).

[3] F. Fernández-Alonso, B. D. Bean, and R. N. Zare, J. Chem. Phys. **111**, 1035 (1999).

[4] F. Fernández-Alonso, B. D. Bean, and R. N. Zare, J. Chem. Phys. **111**, 2490 (1999).

[5] E. Wrede, L. Schnieder, K. H. Welge, F. J. Aoiz, L. Bañares, J. F. Castillo, B. Martínez-Haya, and V. J. Herrero, J. Chem. Phys. **110**, 9971 (1999).

[6] L. Bañares, F. J. Aoiz, V. J. Herrero, M. J. D'Mello, B. Niederjohann, K. Seekamp-Rahn, E. Wrede, and L. Schnieder, J. Chem. Phys. **108**, 6160 (1998).

[7] E. Wrede, L. Schnieder, K. H. Welge, F. J. Aoiz, L. Bañares, V. J. Herrero,

B. Martínez-Haya, and V. S. Rábanos, J. Chem. Phys. **106**, 7862 (1997).
[8] E. Wrede, L. Schnieder, K. H. Welge, F. J. Aoiz, L. Bañares, and V. J. Herrero, Chem. Phys. Lett. **265**, 129 (1997).
[9] E. Wrede and L. Schnieder, J. Chem. Phys. **107**, 786 (1997).
[10] L. Schnieder, K. Seekamp-Rahn, E. Wrede, and K. H. Welge, J. Chem. Phys. **107**, 6175 (1997).
[11] H. Xu, N. E. Shafer-Ray, F. Merkt, D. J. Hughes, M. Springer, R. P. Tuckett, and R. N. Zare, J. Chem. Phys. **103**, 5157 (1995).
[12] L. Schnieder, K. Seekamp-Rahn, J. Borkowski, E. Wrede, K. H. Welge, F. J. Aoiz, L. Bañares, M. J. D'Mello, V. J. Herrero, V. Sáez Rábanos, and R. E. Wyatt, Science **269**, 207 (1995).
[13] N. E. Shafer-Ray, A. J. Orr-Ewing, and R. N. Zare, J. Phys. Chem. **99**, 7591 (1995).
[14] N. E. Shafer, A. J. Orr-Ewing, W. R. Simpson, H. Xu, and R. N. Zare, Chem. Phys. Lett. **212**, 155 (1993).
[15] F. J. Aoiz, M. Brouard, P. A. Enriquez, and R. Sayós, J. Chem. Soc., Faraday Trans. **89**, 1427 (1993).
[16] S. A. Kandel, A. J. Alexander, Z. H. Kim, R. N. Zare, F. J. Aoiz, L. Bañares, J. F. Castillo, and V. S. Rábanos, J. Chem. Phys. **112**, 670 (2000).
[17] W. R. Simpson, T. P. Rakitzis, S. A. Kandel, T. Lev-On, and R. N. Zare, J. Phys. Chem. **100**, 7938 (1996).
[18] W. R. Simpson, A. J. Orr-Ewing, and R. N. Zare, Chem. Phys. Lett. **212**, 163 (1993).
[19] S. A. Kandel, T. P. Rakitzis, T. Lev-On, and R. N. Zare, J. Chem. Phys. **105**, 7550 (1996).
[20] S. A. Kandel, T. P. Rakitzis, T. Lev-On, and R. N. Zare, Chem. Phys. Lett. **265**, 121 (1996).
[21] S. A. Kandel, T. P. Rakitzis, T. Lev-On, and R. N. Zare, J. Phys. Chem. A **102**, 2270 (1998).
[22] A. I. Boothroyd, W. J. Keogh, P. G. Martin, and M. R. Peterson, J. Chem. Phys. **104**, 7139 (1996).
[23] T. C. Allison, R. S. Friedman, D. J. Kaufman, and D. G. Truhlar, Chem. Phys. Lett. **327**, 439 (2000).
[24] S. D. Chao and R. T. Skodje, Chem. Phys. Lett. **336**, 364 (2001).
[25] F. J. Aoiz, L. Bañares, and J. F. Castillo, J. Chem. Phys. **114**, 8237 (2001).
[26] B. K. Kendrick, J. Chem. Phys. **114**, 8796 (2001).
[27] F. Fernández-Alonso, B. D. Bean, J. D. Ayers, D. E. Pomerantz, and R. N. Zare, Z. Phys. Chem. (Munich) **214**, 1167 (2000).
[28] Z. Xu, B. Koplitz, and C. Wittig, J. Phys. Chem. **92**, 5518 (1988).
[29] T. Kinugawa and T. Arikawa, J. Chem. Phys. **96**, 4801 (1992).
[30] P. M. Regan, S. R. Langford, A. J. Orr-Ewing, and M. N. R. Ashfold, J. Chem. Phys. **110**, 281 (1999).
[31] D. Skouteris, J. F. Castillo, and D. E. Manolopoulos, Comput. Phys. Commun. **113**, 128 (2000).
[32] F. J. Aoiz, L. Bañares, and V. J. Herrero, J. Chem. Soc., Faraday Trans. **94**, 2483 (1998).
[33] F. Fernández-Alonso, Ph.D. thesis, Stanford University, 1999.
[34] F. J. Aoiz, V. J. Herrero, O. Puentedura, and V. Sáez Rábanos, Chem. Phys. Lett. **198**, 321 (1992).
[35] D. S. Zakheim and P. M. Johnson, Chem. Phys. **46**, 263 (1980).
[36] D. C. Jacobs and R. N. Zare, J. Chem. Phys. **85**, 5457 (1986).